IEEE Access
Multidisciplinary | Rapid Review | Open Access Journal

Received April 9, 2022, accepted April 24, 2022, date of publication April 28, 2022, date of current version May 9, 2022.

Digital Object Identifier 10.1109/ACCESS.2022.3170910

Experimental Evaluation of Transmitted Signal Distortion Caused by Power Allocation in Inter-Cell Interference Coordination Techniques for LTE/LTE-A and 5G Systems

ÁNGELA HERNÁNDEZ-SOLANA, PALOMA GARCÍA-DÚCAR, ANTONIO VALDOVINOS, JUAN ERNESTO GARCÍA, JESÚS DE MINGO, AND PEDRO LUIS CARRO

Aragon Institute for Engineering Research (I3A), University of Zaragoza, 50018 Zaragoza, Spain

Corresponding author: Ángela Hernández-Solana (anhersol@unizar.es)

This work was supported in part by the Spanish Ministry of Science with European Regional Development Funds (ERDF) under the projects RTI2018-099063-B-I00 and RTI2018-095684-B-I00, and in part by the Government of Aragon (Reference Group T31_20R).

ABSTRACT Error vector magnitude (EVM) and out-of-band emissions are key metrics for evaluating in-band and out-band distortions introduced by all potential non-idealities in the transmitters of wireless systems. As EVM is a measure of the quality of the modulated signal/symbols, LTE/LTE-A and 5G systems specify mandatory EVM requirements in transmission for each modulation scheme. This paper analyzes the influence of the mandatory satisfaction of EVM requirements on the design of radio resource management strategies (RRM) (link adaptation, inter-cell interference coordination), specifically in the downlink (DL). EVM depends on the non-idealities of the transmitter implementations, on the allocated power variations between the subcarriers and on the selected modulations. In the DL of LTE, link adaptation is usually executed by adaptive modulation and coding (AMC) instead of power control, but some flexibility in power allocation remains being used. LTE specifies some limits in the power dynamic ranges depending on the allocated modulation, which ensures the satisfaction of EVM requirements. However, the required recommendations concerning the allowed power dynamic range when inter-cell interference coordination (ICIC) and enhanced ICIC (eICIC) mechanisms (through power coordination) are out of specification, even though the EVM performance should be known to obtain the maximum benefit of these strategies. We perform an experimental characterization of the EVM in the DL under real and widely known ICIC implementation schemes. These studies demonstrate that an accurate analysis of EVM is required. It allows a better adjustment of the design parameters of these strategies, and also allows the redefinition of the main criteria to be considered in the implementation of the scheduler/link adaptation concerning the allocable modulation coding scheme (MCS) in each resource block.

INDEX TERMS EVM, inter-cell interference coordination, LTE, LTE-A, 5G.

I. INTRODUCTION

The error vector magnitude (EVM) and out-of-band emissions resulting from the modulation process are the habitual figures of merit adopted by the 4G/5G (i.e., long term evolution –LTE– standards) for evaluating in-band and out-band distortions introduced in the transmitter communication system and, thus, the signal accuracy of orthogonal frequency division multiple access (OFDMA) transmissions. These distortions limit the signal-to-noise ratio (SNR) in transmission. EVM is the measure of the difference between the ideal modulated symbols and the measured symbols after the equalization (this difference is called the error vector). In order to exploit the full benefit of the modulation, when base stations (named evolved Node B – eNB– in 4G) perform radio resource management (RRM) strategies (i.e., scheduling, link adaptation, and inter-cell interference management), it is important that eNBs take into account not only the

The associate editor coordinating the review of this manuscript and approving it for publication was Tariq Masood.

target block error rate (BLER), linked to the expected signal-to-interference-plus-noise ratio SINR in reception (derived from channel state information –CSI– reported by user equipment –UE–), but also the influence of EVM in the SNR in transmission in order to guarantee that SNR does not degrade too much at the transmitter. In this way, from release 8 to the last specification of 4G/5G standards, specifications have set mandatory and specific EVM requirements for each modulation scheme (QPSK, 16QAM, etc.). Because EVM depends, in addition to several other factors, on the difference in power allocated per subcarrier, satisfaction or EVM requirements must be considered when selecting the modulation coding scheme (MCS) and the transmission power per subcarrier as part of interference management strategies. In fact, this may severely impact the definition of this type of RRM strategies. Specifications set limits linking power and modulation allocation in order to meet mandatory EVM requirements. These limits are defined as the dynamic power range. However, although the required EVM must be fulfilled for all transmit configurations, it is a key aspect that is absent in almost all studies concerning RRM management, which are generally decoupled from radio frequency (RF) transmission analysis [1]–[14]. There are only a very limited number of contributions in which EVM requirements are considered [15]–[18], showing that the performance of the ideal implementations of RRM schemes are severely reduced. However, they do not explicitly analyze EVM. They assume that the dynamic power range defined in the specifications is a mandatory requirement in any scenario to meet the EVM. Nevertheless, we will see that the dynamic power range defined in LTE unnecessarily limits the flexibility of link adaptation in the inter-cell interference (ICI) coordination (ICIC) design, when these ICIC schemes are based on power coordination. The purpose of this study is to analyze the influence of mandatory satisfaction of EVM requirements on RRM design (related to link adaptation and power allocation constraints), specifically when ICIC mechanisms are applied in the downlink (DL). To the best of our knowledge, this aspect has not been previously analyzed in the literature.

QoS in LTE/LTE-A and 5G evolutions depends on RRM strategies, including ICIC and resource and power allocation, operating in an interrelated fashion. By applying rules and restrictions on resource assignments in a coordinated manner between cells concerning the allocable time/frequency resources and the power constraints attached to them, LTE reduces ICI and ensures QoS, particularly at the cell edge.

These schemes are required in both the DL and uplink (UL), but they present differences in the rate (MCS selection) and/or power adaptation according to the link channel conditions and data user requirements.

Power management takes place in both the DL and UL, although the approaches are clearly differentiated. Both conventional and fractional power controls (FPCs) are applied in the UL [19]. The first case is a subcase of the second. Used to limit ICI and to reduce UE power consumption, the aim of UL power control is to fully or partially compensate (when FPC is applied) the path loss to satisfy the SINR requirements of a selected MCS. As a UE should adopt the same MCS and power at all allocated subcarriers, the satisfaction of EVM requirements in transmission (which are the same as in DL [20]) does not translate into restrictions for RRM implementations. EVM depends only on the nonlinearities of the real transmitter chain.

Contrary to the uplink UL, in the downlink DL of LTE/LTE-A systems, to better control interference variations at the UEs in inter-cell scenarios, the first approach and overall goal of downlink power allocation is to budget a constant power spectral density (PSD) for all occupied frequency subcarriers or resource elements (REs) over large time periods. Thus, link adaptation is executed by adaptive modulation and coding (AMC) selection instead of path-loss compensation through power adaptation [19]. A priori, this approach does not preclude the use of ICIC schemes, where frequency coordination aims to reduce ICI by defining different frequency allocation patterns for UEs located in different areas of the cell (for instance, the inner zone and the cell edge) and (in some implementations) by defining different power levels (PSD) on each frequency partition (power coordination). Fig. 1.b1 and Fig. 1.b2 in conjunction with Fig. 1.a illustrate examples of the well-known soft frequency reuse (SFR) and fractional frequency reuse (FFR) schemes, which will be described later. In fact, ICIC derived from FFR and SFR schemes continues to be an important issue to facilitate spatial reuse in both DL [10]–[13] and UL [14] of 5G networks.

Nevertheless, the link quality is not limited only by noise and interference at the receiver, which are the effects considered in almost all the RRM studies. Because of the imperfections of the real transmission chains and because the base station (i.e., evolved Node B –eNB- in LTE) transmits simultaneously to several UEs with different MCS and power levels according to the selected frequency partitions, there are distortion effects that limit the SNR in transmission and, as a result, the maximum SINR achievable in reception. The analysis of these effects, characterized by the EVM measure, must be considered. As mentioned above, according to specifications, a maximum EVM per each modulation level must be guaranteed at the transmitter output. With this aim, from release 8, specifications have set and maintained some limits on the difference between the power of an RE and the average RE power for an eNB at the maximum output power (defined as the dynamic power range [21]) to achieve specific EVM requirements for each modulation scheme (QPSK, 16QAM, 64 QAM, 256 QAM) [21]. However, there are two drawbacks to overcome.

First, almost all the proposals of RRM in the state-of-the-art exclude EVM effects and show the benefits of higher power ranges for the modulation order [15], [6], [7]. Results are obtained under idealized conditions that do not match the actual operation of RF transmitters. Meeting dynamic power range constraints limits the flexibility of using modulations in some power ranges, and drastically degrades the performance

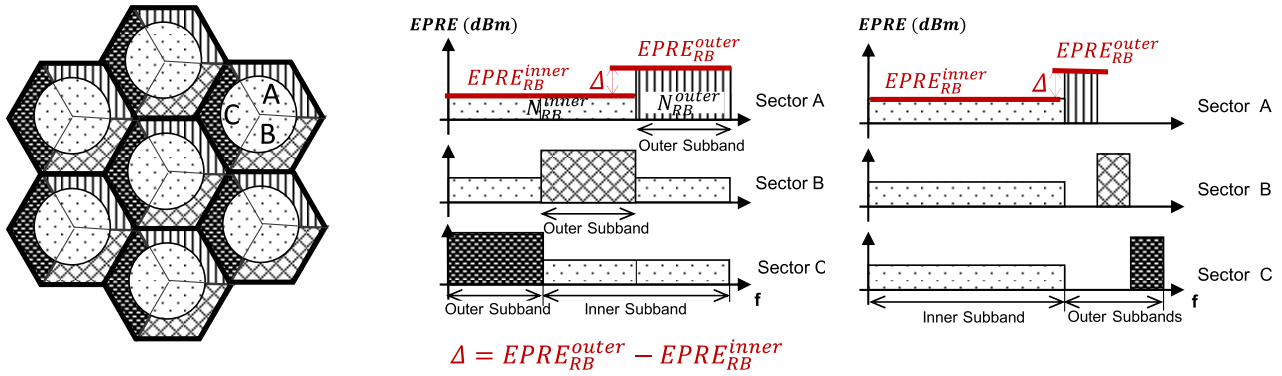

a) Spatial 3-sector site planning and spatial frequency distribution for SFR (b1) and FFR (b2) schemes

b1) Frequency and power allocation for the SFR scheme

b2) Frequency and power allocation for the FFR scheme

FIGURE 1. Inter-cell interference coordination schemes.

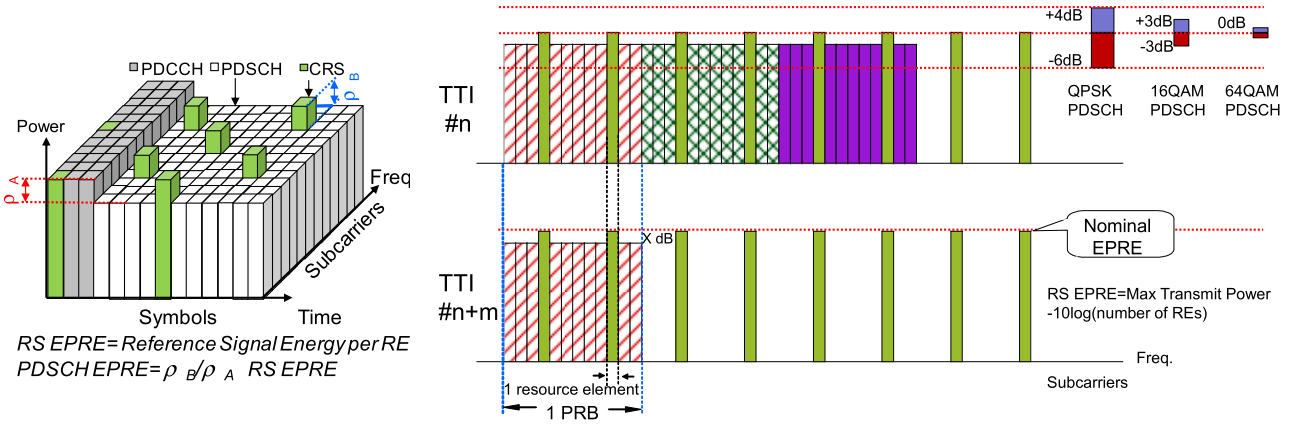

a) Example of downlink power allocation in LTE within a subframe in a PRB

b) Example of evolution of power vs spectral occupation. Definition of E-UTRA BS RE power control dynamic range [21]

FIGURE 2. Resource allocation and downlink power allocation in LTE/LTE-A.

of ICIC schemes [15]–[18] compared with ideal implementation. However, in a second place, these dynamic power range restrictions should be interpreted with caution because they had been defined and suggested under specific conditions and simplified assumptions, because ICIC effects were not included in the studies conducted for the specification.

The EVM depends on many factors related to the implementation of real transmitters. More flexibility in power allocation is possible while meeting EVM requirements, which are considered mandatory. The actual EVM values may be significantly different from those assumed when the standard limits are stated. Contrary to the simplicity of the assumptions used to define the specification, when different power levels are defined in the transmission spectrum mask, different EVM levels can be obtained depending on the location of the RE and not only on the difference of each power level with respect to the average power. These results are useful for improving the resource allocation.

Thus, the objectives of this work are:

1) To emphasize that the proposal and evaluation of RRM strategies, specifically ICIC strategies, need to include mandatory EVM requirements. RRM evaluations that are agnostic of EVM requirements do not properly estimate the actual performance of the proposed schemes. In this context, it is important to note that ICIC and enhanced ICIC (eICIC) based on power coordination remain important ways to facilitate spatial reuse in both downlink and, even, uplink, not only in 4G but also in 5G.
2) To characterize the EVM in the DL transmitter of real RF subsystems, depending on the distribution of modulation and power among subcarriers linked to ICIC and eICIC implementations. The aim is to derive some general performance patterns that allow improving the implementation of these strategies. The objective is to obtain information to be used in the redefinition of the restrictions that must be applied to achieve a better use of resources while meeting the QoS.

First, we concisely review the LTE resource allocation basis and constraints in terms of power allocation defined in the specification while reviewing the expected impact of EVM. Then, the motivation for using some well-known

ICIC and eICIC mechanisms for homogeneous and heterogeneous (HetNet) deployment scenarios schemes is discussed, and the conditioning factors that arise in terms of satisfaction with the EVM requirements are analyzed. Finally, we evaluate the effect of power allocation on the EVM measured over a standard-compliant LTE downlink signal in a real RF subsystem.

II. RELATED WORK

A. DL POWER ALLOCATION ACCORDING TO SPECIFICATIONS

As stated above, conventional power control does not apply to DL, which considers a constant power spectral density for all occupied REs over large time periods and link adaptation through MCS selection.

However, in accordance with this goal, owing to their particular requirements, cell-specific reference signals (CRSs), which are embedded into the overall system bandwidth at certain REs, are transmitted with constant power through all DL system bandwidth and across all subframes. CRSs are involved in several of the most important procedures at the air interface: cell search and initial acquisition, downlink channel quality, reference signal received power (RSRP), reference signal received quality (RSRQ) measurements, and cell (re)selection and measurements for handover support. Therefore, their power level must be constant and known by the UEs, being broadcast in mandatory system information block 2 (SIB2).

DL power management determines the energy (power) per resource element (EPRE). The reference signal (RS) EPRE (RS-EPRE) is easily obtained by dividing the maximum allowed output power ($P^{(p)}_{\max}$) per antenna port (p) in the carrier frequency by the number of REs in the entire bandwidth (see Fig. 2). That is, being the "physical resource block" (PRB) the smallest resource unit that can be scheduled for a UE (which is composed by a number $N^{RB}_{SC} = 12$ of subcarriers in the frequency domain with $\Delta f = 15\ kHz$ subcarrier spacing), the nominal EPRE is obtained by (1):

$$EPRE = E^{(p)}_{\max\_nom} = \frac{P_{\max}}{N^{DL}_{RB} \cdot N^{RB}_{SC}}, \tag{1}$$

being N^{DL}_{RB} the number of PRBs in the downlink bandwidth configuration.

When the RS-EPRE is defined, this parameter is used as a reference to determine the DL EPRE of other DL physical signal components or channels (synchronization signals, broadcast channel –PBCH–, DL control channel –PDCCH–, DL shared channel–PDSCH–, control format indicator channel –PCFICH– and physical hybrid automatic repeat-request indicator channel –PHICH–), whose EPRE (i.e., PDSCH EPRE) is set relative to this value.

Thus, the specification of LTE allows DL power management to allocate different PDSCH EPRE levels. Nevertheless, the ratio of the PDSCH EPRE to cell-specific RS-EPRE among the PDSCH REs (not applicable to PDSCH REs with zero EPRE) should be maintained for a specific condition. This ratio, which depends on the OFDM symbol, is denoted by either ρ_B if the PDSCH RE is on the same symbol where there is an RS (symbol index 0 and 4 of each slot) or ρ_A, otherwise (symbols index 1, 2, 3, 5 and 6) (see Fig. 2a). In our analysis, ρ_A / ρ_B is set to 1.

In addition, the RE power control dynamic range, which is defined as the difference between the power of an RE and the averaged RE power for an eNB at the maximum output power for a specific reference condition (i.e., the threshold of ρ_A and ρ_B), is limited for each modulation scheme used in the PDSCH, according to Table 1 defined in the specification [21] (see Fig. 2.b). In fact, in some specific UE configuration conditions, the allowed ratio ρ_A in OFDM symbols that do not carry RS is limited to eight values (ρ_A is equal to the P_A parameter [22]), ranging from -6 dB to $+3$ dB $\{-6, -4.77, -3, -1.77, 0, 1, 2, 3\}$. Note that in all cases, the output power per carrier should always be less than or equal to the maximum output power of the eNB. This could be considered an additional limitation, but it refers only to signaling. In fact, in release 10 [19], [23], the relative narrowband TX power (RNTP) indicator was exchanged between the eNB through the X2 interface to support dynamic ICIC. The RNTP bit map provides an accurate indication of the power allocation status of each PRB (RNTP (n_{RB}) with $n_{PRB} = 0, \ldots, N^{DL}_{RB} - 1$), taking one of the following values: $\{-\infty, -11, -10, -9, -8, -7, -6, -5, -4, -3, -2, -1, 0, 1, 2, 3\}$. This power status is defined as the ratio between the maximum intended EPRE of the UE-specific PDSCH REs in OFDM symbols that do not contain an RS and the nominal EPRE. Therefore, greater flexibility is considered.

TABLE 1. E-UTRA BS RE power control dynamic range (Table 6.3.1.1-1 in [21]).

Modulation scheme used on the RE	RE power control dynamic range (dB)	
	(down)	(up)
QPSK (PDCCH)	-6	+4
QPSK (PDSCH)	-6	+3
16QAM (PDSCH)	-3	+3
64QAM (PDSCH)	0	0
256QAM (PDSCH)	0	0

TABLE 2. EVM requirements for E-UTRA carrier (Table 6.5.2-1 in [21]).

Modulation scheme for PDSCH	Required EVM [%]
QPSK	17.5 %
16QAM	12.5 %
64QAM	8 %
256QAM	3.5 %

In any case, as stated above, power thresholds are set because the different modulations for the DL (QPSK, 16QAM, 64QAM, and 256QAM) require different limits of EVM to exploit the full benefit of the modulation, and the power control range affects EVM. According to the specifications, the EVM for each modulation of the PDSCH is

better than the values listed in Table 2. The EVM is defined according to (2) as the square root of the ratio of the mean error vector power (difference between the ideal modulated symbols and the measured symbols after equalization) to the mean reference power expressed as a percentage. The EVM measurement shall be performed over all allocated resource blocks and DL subframes within at least 10ms measurement periods. The basic unit of EVM measurement is defined over one subframe (1ms) in the time domain and $N_{BW}^{RB} = N_{SC}^{RB} = 12$ subcarriers (180KHz) as defined in (2) (annex E in [21])):

$$EVM = \sqrt{\frac{\sum_{t\in T}\sum_{f\in F(t)} |Z'(t,f) - I(t,f)|^2}{\sum_{t\in T}\sum_{f\in F(t)} |I(t,f)|^2}}, \tag{2}$$

where T is the set of symbols with the considered modulation scheme being active within the subframe, $F(t)$ is the set of subcarriers within the $N_{\mathrm{BW}}^{\mathrm{RB}}$ subcarriers with the considered modulation scheme being active in symbol t, $I(t,f)$ is the ideal signal reconstructed by the measurement equipment in accordance with relevant transmission (TX) models, and $Z'(t,f)$ is the modified signal under test.

The method for measuring EVM is quite involved (annex E in [21]), but a simple approximation assumes that the error vector resembles white noise. In this case, EVM can be converted to SNR using the following formula: $SNR = 10 \times \log_{10}(1/EVM^2)$. Considering this, the limits in Table 1 were set to meet the EVM requirements defined in the specifications (Table 2) [21]. These values were obtained through simulations to ensure that the system performance was not significantly degraded. Specifically, the dynamic power range was defined for these minimum performance requirements. A range of (7.5% - 8%) EVM was proposed as a working assumption for 64QAM modulated PRBs when PDSCH-EPRE = RS-EPRE. Thus, a better SNR achievable under this condition is 22 dB. To define power range limits, they consider that although there are many causes of EVM, power amplifier (PA) nonlinearities, specifically clipping noise, are the major contributors to EVM. To make the PA implementation efficient, the peak-to-average power ratio (PAPR) of the signal was reduced by clipping the highest peaks. Thus, the signals were slightly modified, indicating this as an additional noise source. The power range was estimated by assuming that if the output power did not change significantly, the clipping noise remained nearly constant and with similar levels for all the PRBs [24]−[26]. Under this assumption, an RE power reduction will lead to a reduced SNR in transmission and a higher EVM that was quantified up to 12.5% (SNR = 18 dB) for 16QAM if the power is reduced by 4 dB and up to 17.5% for QPSK (SNR = 15 dB) with 7 dB of power reduction. By applying a margin, they resulted in −3 dB and −6 dB, as defined in Table 2.

However, these assumptions are not very close to the performance of actual implementations. In addition, because these requirements make the application of many ICIC and eICIC mechanisms difficult (for instance, 64QAM is not allowed in reduced power partitions), a more precise analysis of EVM for ICIC (out of specification) is required to specify enhanced requirements for joint power allocation and modulation selection.

First, as stated above, EVM depends on a number of factors, including thermal noise in various parts of the transmitter chain, precoding, PA linearity, and predistortion characteristics. They are difficult to quantify theoretically, because they depend on vendor implementation. However, apart from the absolute values, general patterns are identified.

1) PA imperfections are the main contributors to EVM, causing a certain loss of signal orthogonality and, thus, a type of in-band interference. This means that even if the total output power does not significantly change by reducing the power of some PRBs while other PRBs are power boosted (as in ICI schemes described next), more degradation is expected to occur when the power is reduced on the selected PRBs. This is because they are more affected by the in-band interference caused by power-boosted PRBs. Therefore, the interference, and thus, this degradation, could not be uniform in all PRBs. This depends on the distance to the power-boosted PRB and the ratio between their respective power levels. The aim of this study is to analyze the EVM degradation depending on the PRB position to improve radio resource allocation.
2) It is a straightforward conclusion that further power reduction beyond the maximum specified power dynamic range can be considered based on the vendor implementation. The EVM could be better than 7.5% for the working point of PDSCH-EPRE = RS-EPRE, and as a result, a power dynamic range could also be defined as the 64QAM meeting EVM requirements. However, in any case, the EVM impact analysis of setting different PDSCH EPRE levels on several PRB partitions on the same OFDM symbol is still necessary.
3) When eICIC mechanisms are applied (reviewed in Section B), normal and low-power (LP) subframes are distributed within a frame (10ms) as shown in Fig. 3. In this case, when a power reduction is applied to all PRBs in an LP subframe, although the channel powers of the cell RS (CRS) and PBCH are maintained to avoid time-variant CRS transmission power fluctuations, the total output power is reduced, and low EVM degradation is expected in these LP subframes compared with subframes when normal operation occurs. It is expected that the PA operates within the saturation limits for normal subframes and applies a power back-off at the PA. In this case, because EVM measurements should be performed within at least 10ms measurements, EVM variations between normal and low-power subframes must be considered in order to ensure EVM requirements in all subframes.

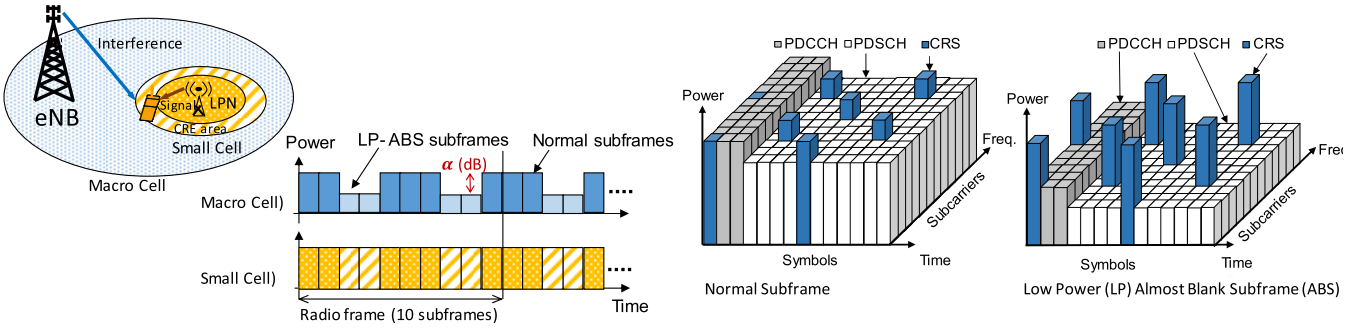

a) Scenario of inter-cell interference coordination in heterogeneous networks (HetNets). Cell Range Expansion (CRE) and eICIC

b) Example of power allocation for normal and Low Power (LP) Almost back Subframes (LP- ABS) at the macro cell.

FIGURE 3. Enhanced Inter-Cell Interference Coordination (eICIC).

B. DL POWER MANAGEMENT AND INTER-CELL INTERFERENCE COORDINATION IMPLEMENTATION

A deeper EVM analysis for ICIC and eICIC may seem unnecessary given the evolution of 4G / 5G systems. However, nothing could be further from the truth.

There are diverse mechanisms to combat inter-cell interference in LTE, including ICI cancellation (IC), ICIC, eICIC mechanisms for the HetNet, coordinated multipoint (CoMP), and coordinated beamforming. A good survey of ICIC techniques can be found in [1]–[4], as well as related radio resource strategies [5] in both standard and heterogeneous LTE/LTE-A networks, along with different performance assessments. To illustrate the impact of EVM on ICIC, it is sufficient to consider two main and well-known categories of ICIC: fractional frequency reuse (FFR) and soft frequency reuse (SFR). FFR and SFR are static ICIC techniques that require interventions from mobile network operators to adjust the PRB and power distribution between cell zones according to UE distribution and quality of service demands. Although simple, these approaches are preferred by many operators, including public safety operators, because of their compatibility with the standard, their inherent ease of implementation, and the fact that they require little or no inter-cell communication. More dynamic implementations are possible by applying dynamic coordination between the eNB. For instance, they are possible using narrow-band transmit power (RNTP) indicator exchange through the X2 interface [2], [3]. In any case, from the early stages of the 4G definition to the present 5G context, a large number of works have studied ICI management based on these low-complexity schemes, resulting in the proposal of many derived variants for 4G and 5G [1]–[5], [8], [10]–[14]. First deployments of 5G networks have been made using OFDMA and proposals for new multiple access techniques are also based on OFDMA, thus, ICIC techniques derived from FFR and SFR remain an important issue to facilitate spatial reuse in both DL [10]–[13] and UL [14].

The basic principle behind these schemes is the division of the available PRBs in the carrier spectrum into two partitions/sub-bands: one intended for mobile users (UE) found in the inner part of the cell and the other that is reserved for users found in the outer or cell-edge area (cell-edge users). Subsequently, several degrees of reuse factors for the inner and outer partitions are applied in a multicell system. In FFR-based approaches, as illustrated in Fig. 1.a with Fig. 1.b2, cell-inner users use the same sub-band in every cell, but the outer sub-band is usually divided into several sub-bands (usually three), and each cell is given a sub-band that is orthogonal to the outer sub-bands in neighboring cells. In this case, the inner region does not share any spectrum with the cell-edge or adjacent cell-edge regions. This strict policy reduces interference on both inner-and cell-edge users but may underutilize the available frequency resources. On the other hand, in SFR-based approaches, the entire bandwidth can be utilized in every cell, and the effective reuse can be adjusted by power coordination between the PRBs used in the inner and outer sub-bands, as illustrated in Fig. 1.a with Fig. 1.b1. Cell-inner users can have access to the cell-edge sub-bands selected by the neighboring cells, but with a lower power level to reduce interference to the neighboring cells. Thus, the SFR achieves higher spectrum efficiency, but there is a higher ICI.

Despite these differences, in all ICIC schemes, there is a common set of basic parameters that must be specified, whose adjustment and optimization have a severe impact on the performance of these schemes [1], [2], [6]–[9]:

1) The set and size of the frequency partitions defined in the PDSCH (e.g., we can identify them as N_{RB}^{inner} and N_{RB}^{edge}).
2) The power level per RE for each frequency partition (e.g., $EPRE_{RB}^{inner}$ and $EPRE_{RB}^{outer}$) and, thus, the power range between them (e.g., $\Delta = EPRE_{RB}^{outer} - EPRE_{RB}^{inner)}$. Note that in partial FFR, different power levels are not strictly needed, although at the edge, sub-band resources can be power-boosted to reach the cell coverage limit.
3) The spatial region where the partitions are used (e.g., cell center or cell edge), and thus, the number of user groups or classes.

4) Threshold criterion for classifying users into groups. Note that FFR and SFR are static/semi-static ICIC techniques, however, they always require interventions in the network to adjust the PRB and power distribution between partitions according to the UE distribution and QoS demands.

Concerning the power level settings, the power in the cell-edge sub-band(s) should be boosted, while the power in the cell-inner sub-band should accordingly be de-boosted to maintain a constant nominal power and maximum output power. Equation (3) sets the expression to compute the power level settings depending on the Δ values that will be used in the evaluation.

$$P_{\max}^{(p)}[mW] = N_{RB}^{inner} \cdot 10^{(12 \cdot EPRE_{RB}^{inner}[dBm]/10)} + N_{RB}^{outer} \cdot 10^{(12 \cdot EPRE_{RB}^{outer}[dBm]/10 + \Delta[dB]/10)} \quad (3)$$

As anticipated, the problem is that if power control dynamic range constraints are required to be satisfied to meet EVM requirements, it is difficult to use or to obtain the maximum benefit of the power control coordination schemes in practical systems. According to Table 1, for instance, if $\Delta > 0$ dB, 64QAM cannot be applied to the SFR or FFR when the outer-cell power boost is also considered, which occurs in most cases. However, almost all state-of-the-art studies until the present have evaluated the performance of their SFR-based or FFR-based proposals without considering these constraints [1]−[13], being the ratio of the outer and inner power densities (Δ) one of the most important parameters in the analysis [1], [2], [6] −[9], [11], [12]. In these studies, 64QAM are frequently used, particularly in the inner sub-bands.

As SFR-based approaches improve spectral utilization, this technique could be particularly effective in some cases; for instance, public safety operators are more affected by limitations on available bands and spectrum bandwidth (3–5 MHz). They often provide support to scenarios with few UE but high resource occupancy. However, the SFR causes more interference to all the center and edge users when compared with the FFR and FFR power-boosted cases. By properly adjusting Δ (for instance, from 0 dB to 10 dB), the operator can control the tradeoff between improving the average cell throughput (low Δ values) and the cell edge throughput (high Δ values). Recently, in [10], the authors propose a flexible soft frequency reuse (F-SFR) that enables a self-organization of a common SFR in the networks with an unpredictable and dynamic topology of flying base stations. Authors propose a graph theory-based algorithm for bandwidth allocation and for a transmission power setting in the context of SFR. They use a deep neural network (DNN) to significantly reduce the computation complexity. However, same as in [8], where a multi-layer SFR is proposed, or [6], [7], [9], where the ratio between the power density in the outer cell region and in the inner cell region is evaluated (from 0 dB to 10 dB or 12 dB), the performance is obtained without considering the effects linked to a real transmitter implementation. Under this assumption, a priori, the dynamic power range is not limited, and the selection of the optimal values, in order to lead to high performance, only depends on the interference caused by co-channel neighbor cells, in addition to RRM (link planning and adaptation) implementations. The same assumptions are applied in the studies conducted in [11], where FFR and SFR with K edge sub-bands are considered and the power ratio ranges from 0 to 20 dB. The same occurs in [12], where authors propose a generalized model of FFR for ultra-dense networks. Knowing that, according to [19], the transmission power in DL should not dynamically change, an FFR scheme extended to N (from 2 to 4) power/frequency sub-bands/groups is proposed. Power levels of each frequency group are appropriately selected to optimize the system operation while the total power consumption remains unchanged. Power ratio between groups varies from 3 to 13 dB, but the optimization does not consider the mandatory requirements of the specifications in order to limit the dynamic power range (linked to power allocation and link adaptation) to meet the error vector magnitude (EVM) requirements at the transmitters. In fact, this is a key aspect that is absent in all the referred studies and in almost all the studies carried out concerning ICI management in DL. All of these studies, and many others available in the literature, are of great interest (i.e., some interesting reviews are available in [1]−[5]). However, a practical limitation of all the proposals is that they do not satisfy the EVM requirements, which has a significant impact on the optimal power allocation, dynamic scheduling, and link adaptation. Considering the interest in ICIC based on power coordination, it is clear that the power control dynamic range must be re-evaluated for ICIC, considering the effects of real transmitter implementations for several values of Δ and MCS distributions among the bandwidth partitions.

To our knowledge, there is only a very limited number of contributions in which satisfaction of EVM requirements is considered (not explicitly but in some way) [15]−[18]. In these contributions, ICIC schemes are proposed and studied in HetNet scenarios, but the problem is similar.

Power control dynamic range defined in Table 1 is imposed in eICIC for HetNet deployments, as illustrated in Fig. 3, where low-power nodes (LPN) are deployed under macrocell coverage. In this case, cell range expansion (CRE) is used to extend the coverage of the LPN, whereas the low power almost blank subframe (LP-ABS) technique is used to decrease the interference caused by the macrocell to the LPN in the extension area (that is, to the cell-edge user in the LPN). LP-ABS is a time-domain ICIC. Contrary to the traditional ABS mechanism, where the macrocell stops its PDSCH transmissions in predefined black subframes intended only for LPN transmissions, in LP-ABS, the macro eNB maintains its data transmissions on the ABS subframes, but the PDSCH EPRE is reduced, with α (where $0 \leq \alpha \leq 1$) the reducing factor. Fig. 3 illustrates the LP-ABS concept with α (e.g. −3 dB). Similar to Δ in ICIC schemes, α is the key design parameter. The studies in [15]−[18] are conducted

from the point of view of RRM design. Thus, the effects of RF implementation are not explicitly considered, but the authors emphasize that the maximum value of allowed power boosting relative to the nominal value must be properly designed to limit the dynamic range and the EVM requirements [21]. In [15], the authors perform a good analysis of the impact of −6 dB, −9 dB, and −12 dB power reductions, concluding that although small values are sufficient to reach the maximum performance in macrocells applying eICIC, larger reductions (i.e., 12 dB) make it possible the application of larger cell range expansion offsets and the consequent improvement of macrocell performance owing to higher picocell offloading ratios. Under ideal conditions (without considering EVM requirements), the same study shows that although it is normal that the modulation order decreases when the transmission power is reduced, a large percentage of 16QAM and 64QAM transmissions are often used in low power subframes. This is because many of these transmissions are directed to the inner UEs, are little affected by interference, and have good channel conditions. However, in [15], when LTE specification constraints (Table 1) are considered, the authors remark that LP-ABS subframes could only be de-boosted to -6 dB from RS-EPRE without significant specification changes, and only if the modulation is constrained to QPSK during these de-boosted subframes. If modulations are limited to QPSK in low-power subframes, as specified, perceptible degradation in the macrocell performance occurs. Increasing the dynamic range (i.e. up to 9 dB) for all the modulations yields in a degradation in the EVM. The same consideration is applied in [16], [17], limiting the power de-boost to 6 dB. They conclude that the support of high power reductions will only be possible at the expense of better EVM requirements for 0 dB to meet the EVM requirements for large power reductions. In a similar way, in [18], where a coordinated multi-point transmission (CoMP) scheduling is applied in combination with ICIC techniques with different power reduction levels, the authors compare the achieved user data rate and system throughput performance without (ideal case) and with LTE constraints (in this case, a dynamic power range is applied and a lower modulation order should be used to conserve modulation accuracy). They show that when the LTE constraints are employed (modulation order is constrained based on the used power offset level), the obtained user data and system throughput performance under the ideal case are drastically degraded regardless of the ICIC technique used. This shows that the LTE constraints should be explicitly considered in any practical RRM proposal. The limitation of all these studies is that they are based on the theoretical power control dynamic range defined in the specifications without an explicit EVM evaluation. However, EVM depends on the vendor implementation and ICIC was out of the studies conducted by the specifications in order to set the dynamic power range.

The only actual limitation is that the EVM for the different modulation schemes in the PDSCH should be better than the limits defined in Table 2. Some power back-offs can be applied to the PA in LP-ABS subframes compared with normal subframes (which impacts the CRS TX power) and need to be evaluated [27]. Thus, the requirements listed in Table 1 must be applied with caution in the LP-ABS. Further power reductions compared with those considered in the dynamic power range can be applied. However, as defined above, the EVM measurements were performed for each PRB within at least 10 measurement periods. This implies that the EVMs from the normal and LP-ABS are averaged. Thus, to ensure a good system performance, the differences between EVMs in PRBs that are not affected by power reductions must be explicitly considered. Concerning the SFR and FFR-based schemes, the most relevant issue is to evaluate the distribution of the EVM along the PRBs in the entire carrier bandwidth according to Δ. Owing to the loss of orthogonality in the transmitted signal caused by many imperfections in the transmitter chain, EVM is expected to vary on the PRBs of the same sub-band depending on their position relative to the boundary between the inner and outer sub-bands. This information can be used in resource allocation, allowing a more precise MCS selection according to the expected EVM on the PRB.

In summary, RRM and RF transmission studies have generally been decoupled in the literature. However, power coordination (linked to ICIC and eICIC), and link adaptation cannot be agnostic to the RF implementation. Being EVM an essential indicator to quantify the transmission performance of a wireless communication, the aim of this work is to quantify the effects in terms of EVM degradation in a real RF subsystem depending on the modulation when power allocation schemes linked to ICIC and eICIC are considered. The kernel of this contribution is that there are no similar studies in the literature. The goal is to avoid unnecessary performance limitations when applying ICIC and eICIC in LTE/LTE-A and 5G cells by restricting the variation range of Δ and α and allocable MCSs. Absolute values depend on vendor implementation, but some generalizable results can be obtained from a detailed study of power coordination linked to ICIC variants derived from the SFR and/or FFR schemes.

III. EXPERIMENTAL RESULTS

In this work, we have carried out an experimental characterization of EVM degradation in a real RF subsystem for several MCS allocations when different power levels are applied as part of the ICIC and eICIC schemes proposed in 4G/5G networks.

To evaluate the effect of power allocation on the EVM measured over the transmitted signal, we have generated a standard-compliant LTE downlink signal (OFDM modulation) with QPSK, 16QAM, and 64QAM modulated subcarriers and a bandwidth of BW = 5 MHz. Thus, a total of 25 PRBs are available. The test signal, generated with MATLAB, which is used in the experiments, follows the LTE frame structure, consisting of different physical signals and channels, including PDSCH, PDCCH, RS, and synchronization data. However, ICIC only applies to the PDSCH; thus, the

power and modulation variation in each PRB is only carried out in the PDSCH.

The power level and MCS can be independently selected for each PRB with the EVM obtained for each PRB. We evaluated different distributions for the inner and outer sub-bands according to the patterns defined for the SFR scheme in sectors A, B, and C (see Fig. 1.a with Fig. 1.b1). The conclusions derived from the results obtained for all the patterns are similar; therefore, without loss of generality, we will include those obtained for pattern C. That is, the outer sub-band is allocated to the first PRB. The two most relevant parameters that affect the EVM are the power ratio between the outer and inner power densities (Δ), defined in Fig. 1, and the distance from the PRB, where the EVM is evaluated as the jump point between the inner and outer sub-bands. Taking this into account and without loss of generality, the results shown here correspond to a scenario in which the sizes of the outer and inner sub-bands are adjusted to be almost equal. That is, $N_{RB}^{inner} = 12$ and $N_{RB}^{outer} = 13$. Power levels are set for different Δ rates according to (2). For example, Fig. 4 shows an LTE frame with 25 PRBs (5 MHz bandwidth), where the first 13 PRBs have a power level 9 dB higher than that of the last 12 PRBs, and a 64-QAM modulation scheme is used for all PRBs.

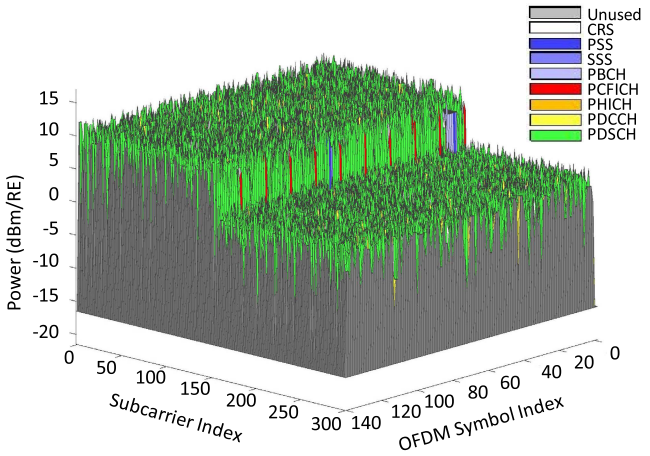

FIGURE 4. Test signal: LTE frame with 25 PRBs where the first 13 PRBs have a power level 9dB higher than the last 12 PRBS (64QAM modulation).

A. EXPERIMENTAL SETUP

The complete experimental test bench is shown in Fig. 5 using an equivalent block diagram. The experimental setup used in this study is shown in Fig. 6.

The digital development platform used for the implementation of digital signal processes and the digital I/Q modulator and demodulator consists of an FPGA Zynq-7000 AP SoC connected to a PC that controls a high-speed analog module with an integrated RF agile transceiver, the Analog Devices AD9361 software defined radio (SDR). It comprises an RF 2×2 transceiver with integrated 12-bit digital analog converters (DACs) and analog to digital converter (ADCs), and

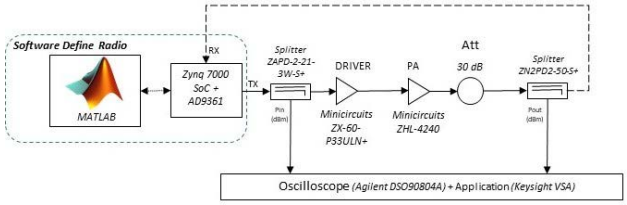

FIGURE 5. Block diagram scheme stands for the experimental setup.

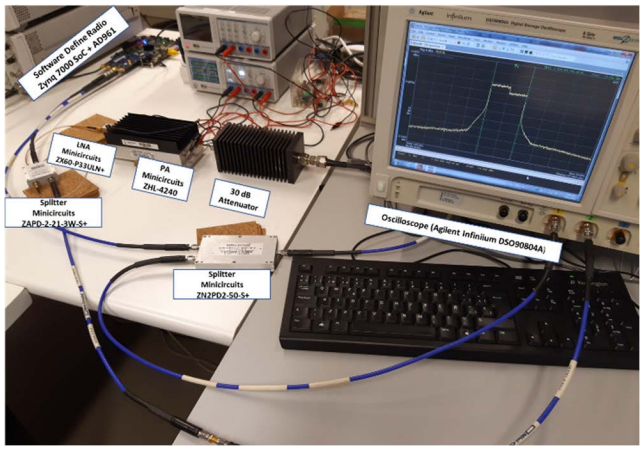

FIGURE 6. Laboratory experimental test setup.

has a tunable channel bandwidth (from 200 kHz to 56 MHz) and receiver (RX) gain control. It is used as a generator and receptor for the LTE signal, as described above. The RF carrier frequency is set at 1.815 GHz within band 3 of the LTE standard [21], which is called DCS.

Because the signal power at the output of the board is low, it is amplified using a low-noise amplifier (LNA) (Minicircuits ZX60-P33ULN+). The signal is then amplified with a PA (Minicircuits ZHL-4240), which has a 1-dB compression point of 26 dBm and an approximate gain of 41.7 dB at the test frequency. As previously stated, the most important cause of the increased EVM level in the transmitted signal is the nonlinear distortion caused mainly by the RF power amplifier (PA), which depends on the operating point of the RF PA. For this reason, in this work, several tests are conducted by varying the operating point of the RF power amplifier, and consequently its RF output power, to evaluate the impact of the nonlinearities of the PA on the EVM level. Fig. 7 shows the amplitude-to-amplitude modulation (AM/AM) characteristics of the RF PA used in the experimental setup at a linear (red dots) and nonlinear (blue dots) operating points, corresponding to an averaged RF output power of 18.4 dBm and 22 dBm, respectively.

The output signal is shown on an oscilloscope (Agilent Infiniium DSO90804A), which measures the signal power. A splitter (Minicircuits ZAPD-2-21-3W-S+) has been added to the setup to measure the signal power before amplification. A second splitter (Minicircuits ZN2PD2-50-S+) is used to capture the amplified output signal and send it to the feedback

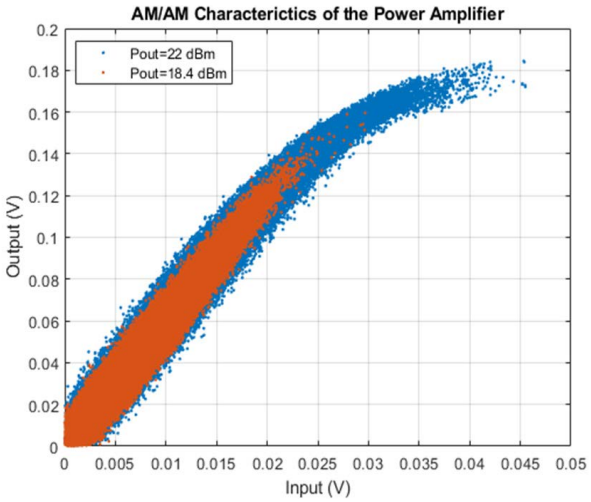

FIGURE 7. AM/AM characteristics of the PA measured in the experimental test setup in a linear and nonlinear scenario.

loop to be demodulated on the board. The demodulation process is carried out on a digital platform and analyzed on a PC with MATLAB. An attenuator of 30 dB is used at the output of the PA to avoid damaging the oscilloscope.

Starting from this testbed, it is known, as we refer above, that the nonlinear distortion caused mainly by the RF power amplifier is the most important cause of increased EVM level in the transmitted signal. Therefore, depending on the operating point of the RF PA, some type of linearization technique may be necessary in a real implementation to reduce the nonlinear distortion produced by the RF power amplifier and thus decrease the EVM level. Therefore, we performed an analysis using a digital predistorter (DPD) included in the system when the PA works in a nonlinear region. DPD processing is performed in the FPGA Zynq-7000 AP SoC, as explained above. In this study, a classical polynomial model based on a truncated Volterra series is chosen for the amplifier model and is defined as (4):

$$y(n) = \sum_{k=1}^{N} \sum_{m=0}^{M} b_{km} x(n-m) \left| x(n-m) \right|^{k-1}, \tag{4}$$

where N is the nonlinear order, M is the memory depth, $x(n)$ and $y(n)$ are the baseband input and output signals, respectively, and b_{km} are the model coefficients.

This model allows us to obtain the DPD characteristics using an indirect learning structure, as explained in [28] and shown in Fig. 8.

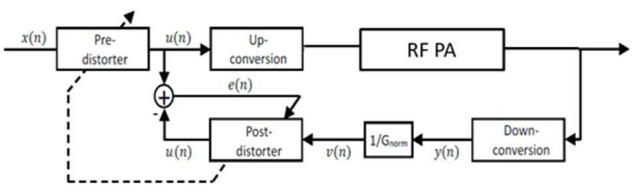

FIGURE 8. Predistorter Scheme using an indirect learning structure.

The predistorted output signal, $u(n)$, is obtained from the baseband input $x(n)$ using (5):

$$u(n) = \sum_{p=1}^{N} \sum_{m=0}^{M} a_{pm} x(n-m) \left| x(n-m) \right|^{p-1}, \tag{5}$$

where M is the memory depth, N is the nonlinear order, m is the memory tap delay, and a_{pm} are the predistorter model coefficients. They are calculated in the first stage of the feedback path (post-distorter), whose input is $v(n)$ and is defined as (6):

$$v(n) = y(n) / G_{norm}, \text{ where } G_{norm} = G_{linRF} = \beta G_{RF}, \tag{6}$$

where G_{linRF} is the linearized RF complex gain, β is the gain factor, and G_{RF} is the complex gain without linearization defined as $G_{RF} = \max |y(n)| / \max |x(n)|$. This factor β is used to compensate for the gain reduction owing to the linearization process.

DPD performance can be improved by carefully adjusting this factor as long as the DPD model remains stable [29]. A more detailed description of this well-known method and how to obtain the input signal matrix expression as well as the coefficient vector can be found in [30]. This model can fit the nonlinearity and memory effects of a power amplifier.

In this study, the DPD parameters, nonlinearity order, and memory depth are fixed (N = 7 and M = 0) for all the downlink RF input signal powers. This corresponds to a basic model without memory, but the aim of this work is not to optimize the DPD but to evaluate the improvement of the EVM with the use of a DPD.

B. RESULTS

A set of experiments has been conducted to evaluate the real effects in terms of EVM degradation in a real RF subsystem considering the MCS allocation, the operating point of the RF PA output power, and the power ratio between the outer and inner power densities (Δ). The final objective is to obtain information to set real restrictions concerning EVM requirements that affect ICIC and eICIC implementations in order to improve resource allocation strategies, including scheduling and link adaptation through MCS selection. As mentioned above, the results presented here correspond to a pattern where the first 13 PRBs correspond to the outer sub-band of an SFR scheme and the last 12 PRBs correspond to the inner sub-band. Similar analyses and equivalent conclusions have been obtained for other patterns of the inner and outer sub-bands and sizes of the sub-bands.

First, Fig. 9 shows the EVM measured in each PRB in various situations depending on the operating point of the RF PA, each of which corresponds to the respective average output power of the PA, with no difference in the power level (Δ = 0 dB) between the inner and outer sub-bands and considering 64 QAM. This allows us to observe the influence of the operating point of the PA on the measured EVM. As expected, the higher the RF output power, the more

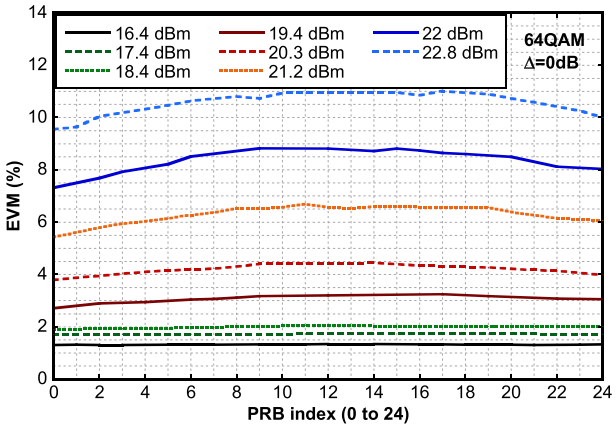

FIGURE 9. EVM measured in each PRB varying the operating point of the RF power amplifier. (Modulation 64QAM and no difference in power level between PRBs $\Delta = 0$ dB).

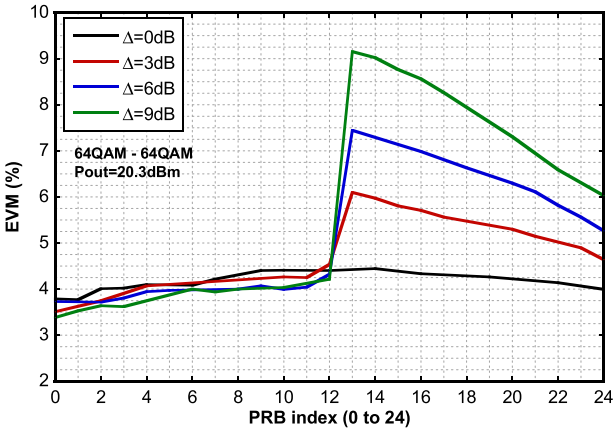

FIGURE 10. EVM measured at an intermediate operating point of the RF PA, corresponding to Pout = 20.3 dBm, varying the power level Δ between the first 13 and the last 12 PRBs from 0 dB to 9 dB. (Modulation 64QAM).

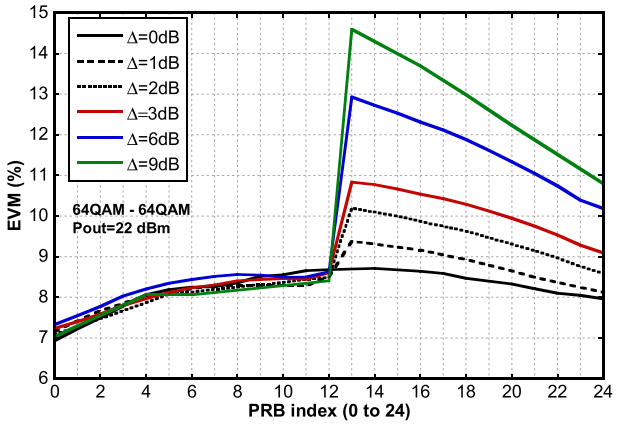

FIGURE 11. EVM measured at a nonlinear operating point of the RF PA, corresponding to Pout = 22 dBm, varying the power level Δ between the first 13 and the last 12 PRBs from 0 dB to 9 dB. (Modulation 64QAM).

nonlinearities in the transmitter, and the higher the EVM value along the whole carrier band.

In addition, Fig. 9 evidences how all the possible nonlinearities in the transmitter lead to the loss of orthogonality between the subcarriers, which generates inter-subcarrier interference (in-band interference), affecting PRBs differently across the band. Because of the decreasing spectral power of individual subcarriers in the side lobes, PRBs located at the edges of the carrier spectrum are affected by a fewer number of interfering subcarriers able to add a significant interference power. Fig. 9 shows this effect: PRBs in the middle of the system band (i.e., PRB#8 to PRB#16) are more affected by the in-band interference and present higher EVM values. Then, EVM decreases slightly at the ends of the band (i.e., PRB#0, PRB#1 or PRB#23, PRB#24). This effect is more significant as the RF PA works in a nonlinear operating point. It should be noted that the EVM requirements of the standard (see Table 2) are not met for higher output power levels. In these cases, it is necessary to include a DPD in the transmitter to meet the specifications for 64QAM (8%).

It is expected that the effect of in-band interference will be more evident when power coordination, linked to SFR, is applied. That is, a power ratio Δ is applied between the outer sub-band (used by the users located in the cell edge) and the inner sub-band (used by the users located in the cell-center). After seeing in Fig. 9 the performance for different points of operation, in Fig. 10 and Fig. 11 we analyze the impact of Δ values in two different points of operation, always considering the more demanding modulation (64QAM) from the EVM point of view. Fig. 10 shows the EVM measured at an intermediate operating point of the RF PA corresponding to Pout = 20.3 dBm, and Fig. 11 shows the EVM measured at a nonlinear operating point corresponding to Pout = 22 dBm. The difference between the power levels of the outer (first 13 PRBs) and inner (last 12 PRBs) sub-bands (Δ) varied from 0 dB to 9 dB.

As expected, the PRBs of the inner sub-band (powered down) will lead to a reduced SNR in transmission and a higher EVM than the PRBs of the outer sub-band. This is why the RE power control dynamic ranges (dB) suggested in the specification depend on the MCS. In addition, we observe that the EVM strongly depends on the distance from the PRB (where the EVM is evaluated) to the jump point between the inner and outer sub-bands. It should be noted that the PRB in the transition zone between the two sub-bands is considerably affected. However, EVM degradation diminished when we moved away from the transition zone. The effect is more noticeable with a larger value of Δ, and for the nonlinear operation point of the RF PA. This is because the in-band interference will affect to a greater extent the subcarriers that are transmitted with less power and are close to others that are transmitted with greater power, because the side lobes of the latter will have a higher relative power with respect to the main lobe of the subcarriers transmitted with less power. This occurs in the transition zone between the inner and outer sub-bands. In this area, the PRBs of the inner sub-band (i.e., PRB#13) suffer more in-band interference level coming from the nearest PRBs of the outer sub-band

(which are power boosted with respect to those of the inner sub-band) than coming from PRBs of the own inner sub-band. This results in an increase of EVM in PRBs of the transition zone (i.e., PRB#13), which decreases in the PRBs as long as they are farther to it. For this reason, as PRB move away from the transition zone in the inner sub-band, the high power subcarriers are further away and affect less, so the PRBs at the band edge (i.e., PRB#23 and PRB#24) will present lower EVM values.

On the contrary, in the outer sub-band, PRBs are affected by the subcarriers of the inner sub-band, which have less power, and by the subcarriers of their own sub-band with similar power. This results in a lower EVM that derives in the corresponding jump between inner and outer sub-bands. Compared with the inner sub-band, EVM appears to remain almost unchanged. However, we see that in the outer sub-band, the EVM increases as we move away from the edge of the carrier band (i.e., PRB#0) to the center because PRBs are affected by more subcarriers adding significant interference on each side. This increase stabilizes when we approach the transition zone (i.e., PRB#12) because subcarriers of the inner sub-band become part of the group of most significant interfering ones and they have less power.

A good characterization of the EVM performance in the inner sub-band will allow us to make suitable decisions at the scheduler concerning the allowed allocable MCS in each PRB. For instance, in Fig. 10, the EVM requirements (8%) are satisfied for $\Delta = 3$ dB and $\Delta = 6$ dB in all PRBs. However, when $\Delta = 9$ dB is budgeted, 64QAM selection is also allowed for PRB#18to PRB#24. In fact, a general indication from the transmitter SNR point of view is to allocate the highest MCS as far as possible from the jump point. As anticipated in Section II, when ICIC strategies are applied, detailed and individualized analyses are required, which are not considered in the standard. Concerning EVM degradation in the low-power sub-band (in this case, the inner-sub-band), it is clear that it depends on the Δ factor. However, the specific relationship between EVM and Δ must be analyzed by considering the transmitter implementation, particularly the actual PA, its operating point, and the use of any linearization technique. The type of analysis that makes it possible to obtain the dynamic power ranges defined in Table 2 cannot be ignored. However, the specific values should not be misunderstood: $\Delta > 0$ does not prevent the use of 64QAM when ICIC and eICIC are applied.

Comparing Fig. 10 and Fig. 11, we can see that the greater the nonlinearity in the transmitter, the greater the difference between the EVM values for PRB#13 and PRB#24.

In Fig. 12, the effect of nonlinearity can be clearly observed. In Fig.12, EVM is measured by varying the operating point of the RF PA when the difference in power level Δ between both sub-bands is set to 6 dB. As shown in Fig. 10 and Fig. 11, there is an increase in the EVM level in the transition zone between the two sub-bands, which decreases as we move away from the transition zone. In this case, it is observed that this effect is more significant when more

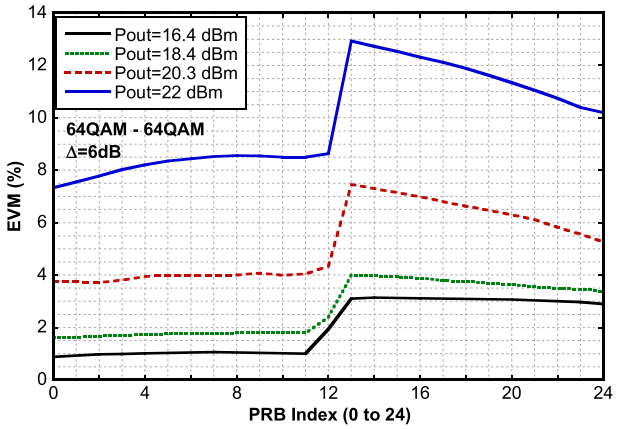

FIGURE 12. EVM measured varying the operating point of the RF power amplifier with a difference in power level $\Delta = 6$dB between the first 13 and the last 12 PRBs. (Modulation 64QAM).

nonlinearities exist in the transmitter, as already observed when we compare Fig. 10 and Fig. 11. In Fig. 11, because the baseline EVM is approximately 8% for $\Delta = 0$ dB, the standard requirements are not satisfied when $\Delta > 0$. In this case, a digital predistorter (DPD) must be included in the transmitter to reduce the measured EVM. When the transmitter works in a more linear zone (i.e., Pout = 16.4 dBm), the non-idealities persist but are less significant, which allows a better preservation of orthogonality. Because of the outer sub-band is power de-boosted, a lower SNR is achieved in the inner sub-band compared to the outer sub-band, resulting in a higher EVM. However, the decreasing effect that occurs when we move away from the transition zone to the edge of the carrier band is almost negligible.

The results of Figs. 9–12 also allow us to infer some relevant conclusions regarding the management of eICIC strategies to combat the interference in HeNet, regardless of the ICIC scheme used in the macrocell to combat inter-cell interference from other macrocells. As mentioned in Section II, it is expected that the PA operates within saturation limits for normal subframes and applies a power back-off at the PA. However, the total output power is also reduced, and a low EVM degradation is expected in these LP subframes compared with subframes where normal operation occurs. If the EVM measurements are performed over a period of at least 10ms, the EVM values are averaged. This means that the EVM requirements can be satisfied in the LP subframes, whereas in normal subframes, it cannot be guaranteed. Thus, the measurements must consider both types of subframes separately. The EVM variations between the normal and low-power subframes should be considered to satisfy the EVM requirements in all subframes.

Taking the working point of the PA that corresponds to a nonlinear zone (Pout = 22 dBm), we want to evaluate the influence of changing the modulation scheme between the inner and outer sub-bands. In Fig. 12, the tests have been performed with 64QAM modulation in all PRBs, whereas

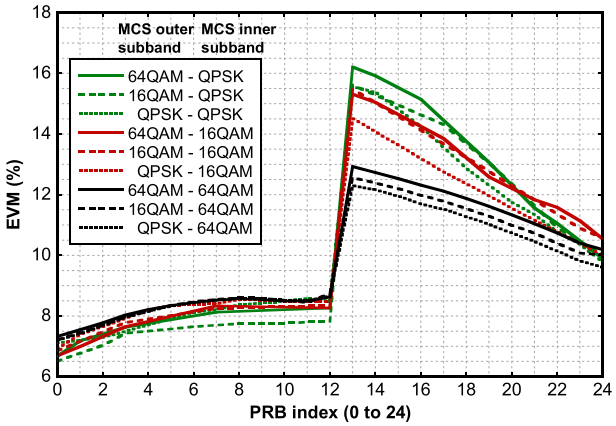

FIGURE 13. EVM measured with different modulations between inner and outer sub-bands (difference in power level $\Delta = 6$dB, Pout = 22 dBm).

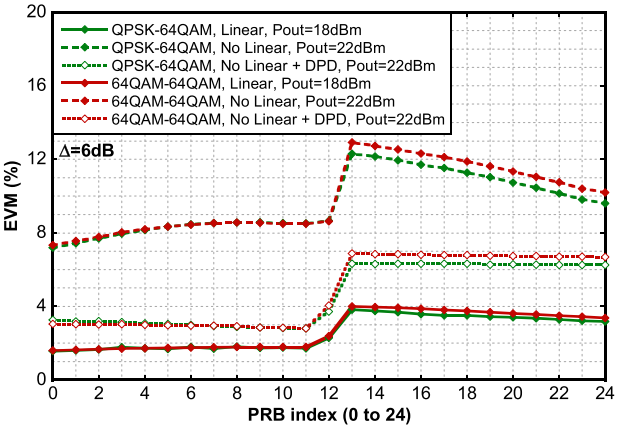

FIGURE 14. EVM measured in a linear (Pout = 18.4 dBm) and nonlinear operating point (Pout = 22 dBm) of the RF PA with and without DPD and with different modulations between inner and outer sub-bands (difference in power level $\Delta = 6$dB).

Fig. 13 shows the results with different modulation schemes. In all cases, an increase in the EVM level appears in the transition zone due to the jump in the power level ($\Delta = 6$ dB), but it is more significant as long as the order of the modulation used in the inner sub-band decreases. For instance, in this specific implementation, when 64QAM is considered in the outer sub-band, in the inner sub-band the EVM increases from 12.9% when 64QAM is used to 15.2 and 16.2% if 16QAM and QPSK are selected, respectively. For a given SNR, the EVM is lower as the modulation order increases. In addition, as SNR increases, the slope of the EVM improvement is larger for the lower modulation orders. In Fig. 13 we see how EVM decreases faster for QPSK as we move away from the transition zone.

Concerning the impact of the MCS used on the outer sub-band, the results are not conclusive; however, in general, the EVM in the inner sub-band decreases as long as a lower modulation is used in the outer sub-band. Related to the EVM in the outer sub-band, slightly lower EVM values are obtained as the EVM grows in the inner band.

Finally, as shown in Fig. 11, in a nonlinear operating point situation of the RF PA, the EVM requirements are

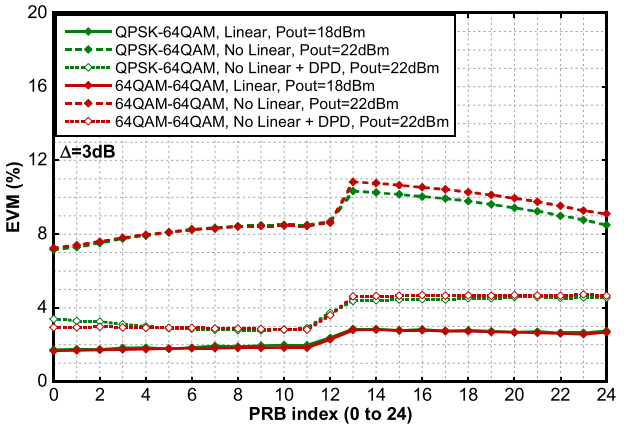

FIGURE 15. EVM measured in a linear (Pout = 18.4 dBm) and nonlinear operating point (Pout = 22 dBm) of the RF PA with and without DPD and with different modulations between inner and outer sub-bands (difference in power level $\Delta = 3$dB).

not satisfied; therefore, a DPD must be included in the transmitter to reduce the measured EVM. To evaluate the effects of the inclusion of a digital predistorter (DPD) at the transmitter, Fig. 14 and 15 show the EVM measured in each PRB at two different operating points of the RF PA: one linear (Pout = 18.4 dBm) and the other nonlinear (Pout = 22 dBm). In both cases, the results have been obtained in two situations: when a QPSK modulation scheme was used in the first 13 PRBs (outer sub-band) and 64QAM in the last 12 PRBs (inner sub-band), and with the same 64QAM modulation scheme in all PRBs. To observe the influence of Δ on the measured EVM, Fig. 14 shows that the first 13 PRBs have a power level $\Delta = 6$ dB higher than the last 12 PRBs, while in Fig. 15, $\Delta = 3$ dB. As in the previous figures, Fig. 14 and Fig. 15 show how a significant increase in the EVM level appears in PRBs 12 and 13 (transition zone), and a decreasing effect as moving away from the transition zone to the edge of the carrier band. This effect is relevant in the nonlinear scenario and is almost negligible in the linear PA and when DPD is applied. In fact, when a DPD is applied, the EVM decreases in all PRBs. For instance, in Fig. 14, EVM reaches values higher than 10% in all the last 12 PRBs when Pout = 22 dBm. When a DPD is applied, EVM decreases in all PRBs below 7%, reaching a value of 3% in the PRBs with a higher power level. The most relevant aspect is that the differences among the PRBs are negligible. Similar conclusions can be obtained from Fig. 15, which shows that the power level difference (Δ) between the inner and outer sub-bands only affects the specific expected EVM values. It can also be observed that in these situations, the influence of the modulation scheme in the EVM is not significant.

IV. CONCLUSION

In this study, we analyzed the influence of mandatory satisfaction of EVM requirements at the transmitter in the design of radio resource management strategies (RRMs) for DL in 4G/5G mobile systems. Specifically, we experimentally analyzed the real effects of the power allocation schemes linked

to ICIC and eICIC in terms of EVM degradation in transmissions. This aspect has not been addressed in studies on ICIC or eICIC, which usually overlook these EVM requirements, resulting in ideal evaluations of RRM proposals and overestimations of the user data transmission and system throughput performance. Only a few works have considered LTE constraints related to the dynamic power range for each modulation order to ensure EVM requirements. However, constraints for ICIC was out of the studies conducted by the specifications. Therefore, the analysis of this work avoids the unnecessary performance limitations that can be achieved when applying ICIC and eICIC in LTE/LTE-A and 5G cells by unnecessarily restricting the range of variation of the allocable power masks and MCSs.

As it is known, the particular numerical results obtained depend on the specific transmitter implementation. Thus, the contribution does not lie in providing a precise numerical quantification of the effects, but in the analysis and verification of some EVM behavior patterns that should be considered to maximize the performance of the ICIC and eICIC schemes while ensuring QoS. We can conclude that the two most relevant parameters that affect the EVM are the power ratio between the outer and inner sub-bands (Δ), PA operation points and the distance from the PRB where the EVM is evaluated to the jump point between the inner and outer sub-bands. It has been shown that the PRB of low-power sub-bands in the transition zone between the two sub-bands is considerably affected by the power jump. However, EVM degradation diminished when we moved away from the transition zone. Future research work could address the design of RRM strategies based on the type of analysis performed in this work. This will allow us to make more suitable decisions at the scheduler concerning the allowed allocable MCS in each PRB.

REFERENCES

[1] A. S. Hamza, S. S. Khalifa, H. S. Hamza, and K. Elsayed, "A survey on inter-cell interference coordination techniques in OFDMA-based cellular networks," *IEEE Commun. Surveys Tuts.*, vol. 15, no. 4, pp. 1642–1670, 4th Quart., 2013.

[2] D. G. González, M. García-Lozano, S. Ruiz, and J. Olmos, "On the need for dynamic downlink intercell interference coordination for realistic long term evolution deployments," *Wireless Commun. Mobile Comput.*, vol. 14, no. 4, pp. 409–434, Mar. 2014.

[3] C. Kosta, B. Hunt, A. U. Quddus, and R. Tafazolli, "On interference avoidance through inter-cell interference coordination (ICIC) based on OFDMA mobile systems," *IEEE Commun. Surveys Tuts.*, vol. 15, no. 3, pp. 973–995, 3rd Quart., 2013.

[4] E. Pateromichelakis, M. Shariat, A. U. Quddus, and R. Tafazolli, "On the evolution of multi-cell scheduling in 3GPP LTE/LTE-A," *IEEE Commun. Surveys Tuts.*, vol. 15, no. 2, pp. 701–717, 2nd Quart., 2013.

[5] Y. L. Lee, T. C. Chuah, J. Loo, and A. Vinel, "Recent advances in radio resource management for heterogeneous LTE/LTE-A networks," *IEEE Commun. Surveys Tuts.*, vol. 16, no. 4, pp. 2142–2180, 4th Quart., 2014.

[6] T. Novlan, R. Ganti, A. Ghosh, and J. Andrews, "Analytical evaluation of fractional frequency reuse for OFDMA cellular networks," *IEEE Trans. Wireless Commun.*, vol. 10, no. 12, pp. 4294–4305, Dec. 2011.

[7] B. M. Hambebo, M. M. Carvalho, and F. M. Ham, "Performance evaluation of static frequency reuse techniques for OFDMA cellular networks," in *Proc. 11th IEEE Int. Conf. Netw., Sens. Control*, Apr. 2014, pp. 355–360.

[8] M. S. Hossain, F. Tariq, G. A. Safdar, N. H. Mahmood, and M. R. A. Khandaker, "Multi-layer soft frequency reuse scheme for 5G heterogeneous cellular networks," in *Proc. IEEE Globecom Workshops (GC Wkshps)*, Dec. 2017, pp. 1–6.

[9] F. Hamdani, A. Maurizka, M. M. Ulfah, and Iskandar, "Power ratio evaluation for soft frequency reuse technique in LTE-A heterogeneous networks," in *Proc. 11th Int. Conf. Telecommun. Syst. Services Appl. (TSSA)*, Oct. 2017, pp. 1–5.

[10] M. S. Hossain and Z. Becvar, "Soft frequency reuse with allocation of resource plans based on machine learning in the networks with flying base stations," *IEEE Access*, vol. 9, pp. 104887–104903, 2021.

[11] A. D. Firouzabadi, A. M. Rabiei, and M. Vehkaperä, "Fractional frequency reuse in random hybrid FD/HD small cell networks with fractional power control," *IEEE Trans. Wireless Commun.*, vol. 20, no. 10, pp. 6691–6705, Oct. 2021.

[12] S. C. Lam and X. N. Tran, "Fractional frequency reuse in ultra dense networks," *Phys. Commun.*, vol. 48, Oct. 2021, Art. no. 101433.

[13] Z. H. Abbas, M. S. Haroon, F. Muhammad, G. Abbas, and F. Y. Li, "Enabling soft frequency reuse and Stienen's cell partition in two-tier heterogeneous networks: Cell deployment and coverage analysis," *IEEE Trans. Veh. Technol.*, vol. 70, no. 1, pp. 613–626, Jan. 2021.

[14] H. Carvajal, N. Orozco, D. Altamirano, and C. De Almeida, "Performance analysis of non-ideal sectorized SFR cellular systems in rician fading channels with unbalanced diversity," *IEEE Access*, vol. 8, pp. 133654–133672, 2020.

[15] B. Soret and K. I. Pedersen, "Macro transmission power reduction for HetNet co-channel deployments," in *Proc. IEEE Global Commun. Conf. (GLOBECOM)*, Dec. 2012, pp. 4126–4130.

[16] B. Soret, A. D. Domenico, S. Bazzi, N. H. Mahmood, and K. I. Pedersen, "Interference coordination for 5G new radio," *IEEE Wireless Commun.*, vol. 25, no. 3, pp. 131–137, Jun. 2018.

[17] B. Soret and K. I. Pedersen, "On-demand power boost and cell muting for high reliability and low latency in 5G," in *Proc. IEEE 85th Veh. Technol. Conf. (VTC Spring)*, Jun. 2017, pp. 1–5.

[18] T. Cogalan, S. Videv, and H. Haas, "Coordinated scheduling for aircraft in-cabin LTE deployment under practical constraints," in *Proc. IEEE 87th Veh. Technol. Conf. (VTC Spring)*, Jun. 2018, pp. 1–6.

[19] *Evolved Universal Terrestrial Radio Access (E-UTRA); Physical Layer Procedures*, document TS-36.213 V14.16.0, 3GPP, Release 14, Sep. 2020.

[20] *Evolved Universal Terrestrial Radio Access (E-UTRA); User Equipment (UE) Radio Transmission and Reception*, document TS 36.101 V14.22.0, Release 14, 3GPP, Mar. 2022.

[21] *Evolved Universal Terrestrial Radio Access (E-UTRA); Base Station (BS) Radio Transmission and Reception*, document TS 36.104 V14.10.10, Release 14, 3GPP, Mar. 2021.

[22] *Evolved Universal Terrestrial Radio Access (E-UTRA); Radio Resource Control (RRC) Protocol Specification*, document TS 36.331 V14.16.0, Release 14, 3GPP, Jan. 2021.

[23] Y. Wang, W. Zhang, F. Peng, and Y. Yuan, "RNTP-based resource block allocation in LTE downlink indoor scenarios," in *Proc. IEEE Wireless Commun. Netw. Conf. (WCNC)*, Apr. 2013, pp. 334–3341.

[24] *Proposal for eNB TX Dynamic Range Requirements*, document R4-080113, Nokia Siemens, 3GPP TSG-RAN Working Group 4 Meeting #46, Sorrento, Italy, Feb. 2008.

[25] *BS TX Dynamic Range*, document R4-080038, TP for 36.104, NTT DoCoMo, NXP, 3GPP TSG-RAN Working Group 4 Meeting #46, Sorrento, Italy, Feb. 2008.

[26] *BS TX Dynamic Range, Panasonic*, document R4-080084, 3GPP TSG RAN WG4 (Radio) Meeting #46, Sorrento, Italy, Feb. 2008.

[27] *LS on BS Implications Due to LP-ABS for feICIC*, document R4-122088, Huawei, HiSilicon, 3GPP TSG-RAN WG4 Meeting #62, Jeju, South Korea, Mar. 2012.

[28] C. Eun and E. J. Powers, "A new Volterra predistorter based on the indirect learning architecture," *IEEE Trans. Signal Process.*, vol. 45, no. 1, pp. 223–227, Jan. 1997.

[29] A. Zhu, P. J. Draxler, J. J. Yan, T. J. Brazil, D. F. Kimball, and P. M. Asbeck, "Open-loop digital predistorter for RF power amplifiers using dynamic deviation reduction-based Volterra series," *IEEE Trans. Microw. Theory Techn.*, vol. 56, no. 7, pp. 1524–1534, Jul. 2008.

[30] L. Ding, G. T. Zhou, D. T. Morgan, Z. Ma, J. S. Kenney, J. Kim, and C. R. Giardina, "A robust digital baseband predistorter constructed using memory polynomials," *IEEE Trans. Commun.*, vol. 52, no. 1, pp. 159–165, Jan. 2004.

ÁNGELA HERNÁNDEZ-SOLANA received the degree in telecommunications engineering and the Ph.D. degree from the Universitat Politècnica de Catalunya (UPC), Spain, in 1997 and 2005, respectively. She has been working at UPC and the University of Zaragoza, where she has been an Associate Professor, since 2010. She is a member of the Aragón Institute of Engineering Research (I3A). Her research interests include 5G/4G technologies, heterogeneous communication networks and mission-critical communication networks, with emphasis on transmission techniques, radio resource management and quality of service, mobility management and planning, and dimensioning of mobile networks.

PALOMA GARCÍA-DÚCAR was born in Zaragoza, Spain, in 1972. She received the degree in telecommunications engineering and the Ph.D. degree from the University of Zaragoza, in 1996 and 2005, respectively. In 1995, she was employed at Teltronic, S.A.U., where she worked with the Research and Development Department, involved in the design of radio communication systems (mobile equipment and base station), until 2002. From 1997 to 2001, she has collaborated in several projects with the Communication Technologies Group, Electronics Engineering and Communications Department, University of Zaragoza. In 2002, she joined the Centro Politécnico Superior, University of Zaragoza, where she is currently an Assistant Professor. She is also involved as a Researcher with the Aragon Institute of Engineering Research (I3A). Her research interests include the area of linearization techniques of power amplifiers and signal processing techniques for radio communication systems.

ANTONIO VALDOVINOS received the degree in telecommunications engineering and the Ph.D. degree from the Universitat Politècnica de Catalunya (UPC), Spain, in 1990 and 1994, respectively. He was with UPC and the University of Zaragoza, where he has been a Full Professor, since 2003. He is a member of the Aragón Institute of Engineering Research (I3A). His research interests include 5G/4G technologies, heterogeneous communication networks and mission-critical communication networks, with emphasis on transmission techniques, radio resource management and quality of service, mobility management, and planning and dimensioning of mobile networks.

JUAN ERNESTO GARCÍA was born in Zaragoza, Spain, in 1997. He received the bachelor's and master's degrees in telecommunications engineering from the University of Zaragoza, in 2019 and 2021, respectively. In 2020, he was employed with the Communication Technologies Group, Department of Electronics Engineering and Communications, University of Zaragoza, after collaborating with them during the final bachelor's degree thesis, where he worked in the research of several lineralization techniques for critical mobile communication systems. In 2021, he joined Indra Sistemas S. A., where he is currently working in the Solution and Product Area as a System Engineer. He is still collaborating as a Researcher with the Aragon Institute of Engineering Research (I3A). His research interests include the area of radio-frequency design and signal processing techniques for critical radio communication systems.

JESÚS DE MINGO was born in Barcelona, Spain, in 1965. He received the Ingeniero de Telecomunicación degree from the Universidad Politécnica de Cataluña (UPC), Barcelona, in 1991, and the Doctor Ingeniero de Telecomunicación degree from the Universidad de Zaragoza, in 1997. In 1991, he joined the Antenas Microondas y Radar Group, Departamento de Teoría de la Señal y Comunicaciones, until 1992. In 1992, he was employed at Mier Comunicaciones, S.A., where he worked in the solid state power amplifier design, until 1993. Since 1993, he has been an Assistant Professor, since 2001, an Associate Professor, and since 2017, a full Professor with the Departamento de Ingeniería Electrónica y Comunicaciones, Universidad de Zaragoza. He is a member of the Aragon Institute of Engineering Research (I3A). His research interests include the area of linearization techniques of power amplifiers, power amplifier design, and mobile antenna systems.

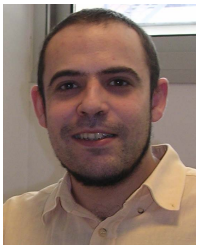

PEDRO LUIS CARRO was born in Zaragoza, Spain, in 1979. He received the M.S. degree in telecommunication engineering and the Ph.D. degree from the University of Zaragoza, in 2003 and 2009, respectively. In 2002, he carried out his master thesis on antennas for mobile communications at Ericsson Microwave Systems, A.B., Göteborg, Sweden, with the Department of GSM and Antenna Products. From 2002 to 2004, he was employed at RYMSA S.A., where he worked with the Space and Defense Department as an Electrical Engineer, involved in the design of antennas and passive microwave devices for satellite communication systems. From 2004 to 2005, he worked with the Research and Development Department, Telnet Redes Inteligentes, as a RF Engineer, involved in radio over fiber systems. In 2005, he joined the University of Zaragoza, as an Assistant Professor with the Electronics Engineering and Communications Department. His research interests include the area of mobile antenna systems, passive microwave devices, and power amplifiers.